Synchronously pumped laser without inversion in cadmium

de Jong, F.B.; Mavromanolakis, A.; Spreeuw, R.J.C.; van Linden van den Heuvell, H.B.

DOI
10.1103/PhysRevA.57.4869
Publication date
1998

Published in
Physical Review A

Synchronously pumped laser without inversion in cadmium

F. B. de Jong, A. Mavromanolakis, R. J. C. Spreeuw, and H. B. van Linden van den Heuvell
Van der Waals-Zeeman Institute, University of Amsterdam, Valckenierstraat 65, 1018 XE Amsterdam, The Netherlands
(Received 8 January 1998)

We report a lasing without inversion (LWI) experiment on the basis of coherent population trapping, realized in low-pressure cadmium vapor. A single-pass inversionless amplification by more than a factor of 10 has been measured, a significant improvement over previous experiments. In addition, we report synchronously pumped laser oscillation without inversion. Using a simple model to fit the gain/absorption curves as a function of magnetic field, we have obtained values for the populations in the system, showing that there is no inversion in the atomic basis. Combined with a simple optical method to measure absolute densities of a gas, this model results in a completely optical method to determine the absolute populations and density in the system. [S1050-2947(98)03106-0]

PACS number(s): 42.50.Gy, 32.80.Qk, 42.55.−f

I. INTRODUCTION

The topic of lasing without inversion (LWI) has attracted a lot of attention for quite some time, because of the possible applications in short-wavelength lasing. Due to the ω^3 dependence of the Einstein A coefficient, transitions with larger energy splitting generally have faster decay processes which makes it more difficult to create inversion using conventional incoherent pumping. The study of atomic coherence in laser schemes has led to many suggestions for LWI schemes. In this paper we report a laser oscillation experiment in a coherent population trapping scheme.

Since the original theoretical work [1–3] and amplification experiments [4–6] many theoretical contributions have followed and new experiments showing actual lasing without inversion have been reported [9,10]. Studies on lasing without inversion [11–14] show that two kinds of schemes can be identified:

(1) Schemes based on coherent population trapping where a hidden inversion can be revealed by a basis transformation. Most of the experimental work has concentrated on these coherent population trapping schemes but so far only amplification without inversion has been reported [4–8].

(2) Schemes that are inversionless in the sense that there is no atomic basis for which inversion can be found. Laser action has been reported in a V-type level structure for Rb [9] and in a Λ-level structure for Na [10]. The V scheme has recently been discussed in terms of the quantum Zeno effect [15].

The experiments reported in this paper belong to the first type of schemes and are an extension of previous work on inversionless *amplification* in Cd [6]. In that experiment single nanosecond pulses were used. In the present experiment the use of pulse trains and shorter optical pulses (picosecond pulses) has made inversionless *laser oscillation* possible in the same cadmium system.

II. INVERSIONLESS AMPLIFICATION AND LASING IN CADMIUM

We consider inversionless amplification and laser action between the $^3S_1$ state and the $^3P_1$ state in cadmium; see Fig. 1. By inversionless we mean that at all times $N_{^3S_1} \leq N_{^3P_1}$, where N denotes the dimensionless population fraction of a level, irrespective of the distribution over its magnetic sublevels. In a coherently pumped two-level system inversionless lasing is possible on the Rabi-side bands; see Ref. [16] and references therein. Inversionless lasing between *two* incoherently pumped levels is impossible. A similar strong statement cannot be made for systems that involve more than two levels. In the present experiment we use the Zeeman substructure of the $^3P_1$ state to create an amplification condition for a pulsed optical field. We will use the notation $|-\rangle$, $|0\rangle$, $|+\rangle$ for the $m_J=-1,0,1$ sublevels of the $^3P_1$ state, and $|u\rangle$ for the $m_J=0$ sublevel of the $^3S_1$ state. Simultaneous excitation of the magnetic sublevels $|-\rangle$ and $|+\rangle$ of the $^3P_1$ state [see Fig. 2(a)] generates a coherence ρ_{+-} between these levels, responsible for the cancellation of absorption (induced transparency), which makes inversionless amplification possible.

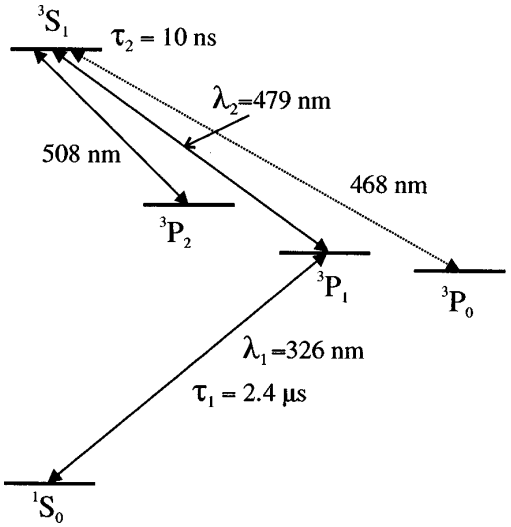

FIG. 1. Wavelengths and lifetimes of atomic cadmium states involved in the experiment. The population of the upper $^3S_1$ state is monitored by detecting the fluorescence decay to the $^3P_2$ state. The wavelength of this fluorescence, 508 nm, is the longest wavelength in the experiment and is easily selected by filtering.

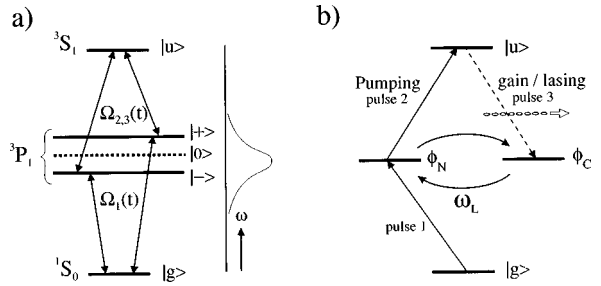

FIG. 2. (a) States coupled by the optical fields in the atomic eigenbasis. The bandwidth of the optical excitation pulse is larger than the frequency splitting between the magnetic sublevels $|-\rangle$ and $|+\rangle$. (b) Superposition states in the cadmium $^3P_1$ state. Simultaneous excitation of the magnetic sublevels of the $^3P_1$ state leads to a coherent superposition, $|\phi_N\rangle=|-\rangle-|+\rangle$. In the basis of superposition states $|\phi_N\rangle$ couples only to the pumping pulses and not to the probe or laser field; $|\phi_C\rangle$ couples to the probe (or laser field) but not to the pump pulses. The total population of the $^3P_1$ preforms a Larmor precession between the $|\phi_N\rangle$ and $|\phi_C\rangle$ states.

The experiment is divided in three steps. The first, linearly polarized excitation pulse [pulse 1, in Fig. 2(b)] prepares a coherent superposition $|\phi_N\rangle=(1/\sqrt{2})(|-\rangle-|+\rangle)$ of the Zeeman sublevels of the $^3P_1$ state. We call the orthogonal superposition state $|\phi_C\rangle=(1/\sqrt{2})(|-\rangle+|+\rangle)$; see Fig. 2(b). Initially only $|\phi_N\rangle$ is populated but the $^3P_1$ states start to perform a Larmor precession in a magnetic field; the $^3P_1$ population oscillates back and forth between $|\phi_N\rangle$ and $|\phi_C\rangle$. After a delay time a second pulse with linear, orthogonal polarization excites part of the available $|\phi_N\rangle$ population to the upper $^3S_1$ state. Only the magnetic sublevel $m_J=0$ of the upper state is populated. Immediately after the second pulse a third pulse arrives with polarization parallel to the first pulse. This third pulse probes the population difference between the $^3S_1$ state and $|\phi_C\rangle$ and can be either attenuated or amplified.

III. REVEALING THE HIDDEN INVERSION

The role of coherences in a three-level laser scheme can easily be described using the semiclassical density matrix formalism [17]. Using the Bloch equations we will show how a coherence between $|-\rangle$ and $|+\rangle$ can overcome the lack of inversion between the $^3S_1$ and $^3P_1$ states. Consider the propagation of a short optical probe pulse (pulse 3 in the experiment) with a carrier frequency ω, resonant with the $|u\rangle\leftrightarrow|0\rangle$ transition, ω_0. Since the polarization is linear and the bandwidth of this pulse is larger than the Larmor frequency splitting, the field interacts with both the $|u\rangle\leftrightarrow|-\rangle$ and $|u\rangle\leftrightarrow|+\rangle$ transition coherently; see Fig. 2(a). We will use the notation $\Omega_3(z,t)$ for the pulse envelope expressed as a Rabi frequency [$\Omega_3(z,t)$ is slowly varying compared to the carrier frequency ω], and 2Δ for the Larmor frequency splitting between levels $|-\rangle$ and $|+\rangle$. Ignoring the decay of the $^3P_1$ state ($\tau_{\text{pulse}}\ll\tau_1$) the Bloch equations for the upper-state population and coherences are (in the rotating-wave approximation and after transforming to the rotating frame)

$$\frac{\partial\rho_{uu}}{\partial t}=-\frac{1}{\sqrt{2}}\Omega_3[\mathrm{Im}(e^{-i\Delta t}\rho_{u-})+\mathrm{Im}(e^{i\Delta t}\rho_{u+})], \quad (1)$$

$$\frac{\partial\rho_{u-}}{\partial t}=\frac{i}{2\sqrt{2}}e^{i\Delta t}\Omega_3(\rho_{uu}-\rho_{--})-\frac{i}{2\sqrt{2}}e^{-i\Delta t}\Omega_3\rho_{+-}, \quad (2)$$

$$\frac{\partial\rho_{u+}}{\partial t}=\frac{i}{2\sqrt{2}}e^{-i\Delta t}\Omega_3(\rho_{uu}-\rho_{++})-\frac{i}{2\sqrt{2}}e^{i\Delta t}\Omega_3\rho_{-+}. \quad (3)$$

The factor $1/\sqrt{2}$ appearing in front of Ω_3 is a consequence of the decomposition of linearly polarized light into a superpositin of left-handed and right-handed circularly polarized light. When the probe pulse $\Omega_3(z,t)$ arrives the populations $\rho_{uu},\rho_{--},\rho_{++}$ and the coherences ρ_{+-},ρ_{-+} have been given an initial value by the pump pulses. Although the pump pulses also create coherences ρ_{u-} and ρ_{u+} the probe beam cannot interact with these coherences since the pump pulse 2 and the probe pulse 3 make a small angle and are therefore not phase matched. So we assume $\rho_{u-}(t=0)=\rho_{u+}(t=0)=0$. This three-level system is inversionless, ρ_{uu} is smaller than ρ_{--} or ρ_{++}. The probe field is amplified if its interaction with the atomic system reduces the upper state population, ρ_{uu}. The equations show that the transfer of upper-state population into gain of the optical pulse is proportional to $\mathrm{Im}(e^{-i\Delta t}\rho_{u-}+e^{i\Delta t}\rho_{u+})$. Without preparation of an initial coherence ρ_{+-} the coherences ρ_{u-} and ρ_{u+} are created from the population terms proportional to $(\rho_{uu}-\rho_{--})$ and $(\rho_{uu}-\rho_{++})$, which only contribute to gain if there is inversion. If, however, a coherence ρ_{+-} is prepared before the pulse interacts with the system, gain becomes possible even without inversion. For a short probe pulse, we have $e^{\pm i\Delta t}=1$ so that a real and negative initial coherence ρ_{+-} will lead to gain without inversion if (assuming Ω_3 is real and positive)

$$|\rho_{+-}|>|\rho_{uu}-\rho_{--}|, \quad |\rho_{uu}-\rho_{++}|, \quad (4)$$

meaning that the lack of inversion in Eq. (2) and Eq. (3) is overcome by the coherence term. This is a general signature of all LWI schemes.

The LWI scheme presented here contains hidden inversion as can be revealed by a simple basis transformation. This leads to a simpler picture of the physical processes. We transform to a basis of superposition states of the magnetic sublevels $|-\rangle$ and $|+\rangle$ [see Fig. 2(b)]

$$|\phi_C\rangle=\frac{1}{\sqrt{2}}(|-\rangle+|+\rangle), \quad |\phi_N\rangle=\frac{1}{\sqrt{2}}(|-\rangle-|+\rangle). \quad (5)$$

Horizontally polarized light of 479 nm (pulse 3) interacts with the coupled state $|\phi_C\rangle$, and will have no interaction with the noncoupled state, $|\phi_N\rangle$, while vertically polarized light of 479 nm (pulse 2) interacts with only the noncoupled state $|\phi_N\rangle$. In the new basis the Bloch equations for the three-level system $|u\rangle$, $|-\rangle$, $|+\rangle$ reduce to two-level equations for the $|u\rangle$ and $|\phi_c\rangle$ states:

$$\frac{\partial\rho_{uu}}{\partial t}=-\Omega_3\ \mathrm{Im}(\rho_{uc}), \quad (6)$$

$$\frac{\partial \rho_{uc}}{\partial t} = \frac{i}{2}\Omega_3(\rho_{uu} - \rho_{cc}). \tag{7}$$

These are simply the usual Bloch equations for two states, $|u\rangle$ and $|\phi_C\rangle$, coupled by an optical field $\Omega_3(z,t)$. The probe can only be amplified if an initial inversion $\rho_{uu} - \rho_{cc}$ is prepared by the pump pulses. Note that such initial inversion is indeed created in our experiment. The population of the $^3P_1$ state is hidden in the $|\phi_N\rangle$ state, which is decoupled from the probe field.

In further analysis of the gain and laser oscillation experiments we will use this simple two-level nature of the coupling of probe field (or laser field) to the atomic system.

IV. EXPERIMENTAL SETUP

The setup consists of two synchronously pumped pulsed dye lasers operating at 652 nm and 479 nm, at a repetition rate of 10 Hz. We use a mode-locked Nd:YAG pump laser producing a train of approximately 8 pulses of duration 40 ps, with 7.1 ns between the pulses. Part of the pulse train is amplified to 18 mJ per train, the remainder passes a pulse slicer and is amplified as a single pulse to 15 mJ per pulse. The frequency doubled and tripled pulse *trains* at 532 and 355 nm are used to synchronously pump two dye oscillators [18] at 652 and 479 nm, respectively. Both lasers have a 1-mm intracavity etalon that limits the bandwidth of the pulses to 30 GHz.

The *single* pulse produced by the Nd:YAG pump laser is also frequency doubled and tripled and is used to amplify one pulse out of the dye oscillator pulse trains. The 652-nm laser uses DCM dye dissolved in methanol for the oscillator, a transverse amplifier, and a longitudinally pumped amplifier, and gives about 60 μJ. The output is frequency doubled to excite the 326-nm transition to the $5s5p\ ^3P_1$ state and is referred to as pulse 1, with an energy of approximately 1 μJ. The 479-nm laser uses Coumarine 102 dissolved in methanol. The pulse energy after the single transverse amplifier is approximately 10 μJ. This second pulse (479 nm) has a fixed delay with respect to the first excitation pulse (326 nm) of 3 (10 ns). The third, ''probe'' pulse (479 nm) is split off from the second pulse, reduced in intensity by three crossed polarizers, and is spectrally filtered to a bandwidth of 2 GHz using a 1-mm etalon with 95% reflectivity. Its polarization is perpendicular to the second, ''pump'' pulse. The pulse duration of the amplified dye-laser pulses is 35 ps.

The atomic vapor of the enriched cadmium-112 isotope is contained in a 10-cm-long quartz cell, which is heated inside an oven to 225 °C. The density of the atomic vapor is adjusted by changing the temperature of the cell. A magnetic field is supplied by two coils of 1-m diameter in a Helmholtz configuration, giving a homogeneous magnetic field over the length of the cell. The field is directed along the propagation axis of the beams; see Fig. 3. A photomultiplier tube (PMT 1) monitors the fluorescence through a 1-cm-diameter pipe, from the atoms in the middle of the 10-cm cell. The photomultiplier tube is placed outside the large coils to avoid disturbance by the magnetic field.

The first excitation pulse (326 nm) and the third (probe) pulse (479 nm) have the same linear polarization and they overlap spatially. The second excitation pulse (479 nm) has orthogonal polarization and makes a small angle with the other pulses allowing us to spatially separate it from the probe pulse after passing the cell. A small prism disperses the overlapping first excitation pulse and probe pulse. The probe is detected by a second photomultiplier tube (PMT 2) after passing two pinholes and a polarizer to eliminate stray light of the second pump pulse. All three beams have a diameter of 2 mm and are copropagating inside the cell. The interaction volume is 0.3 cm^3.

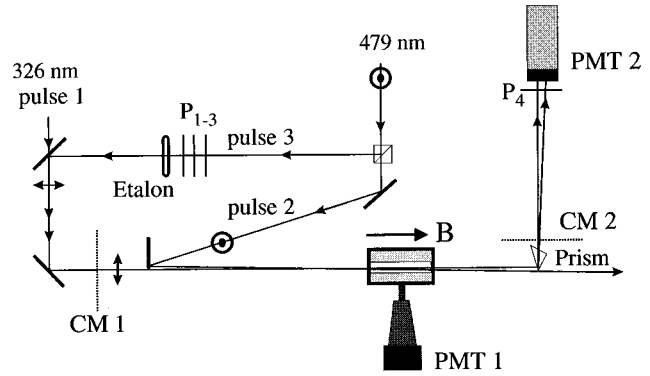

FIG. 3. Experimental setup. The 479-nm pulse is delayed over 3 m (10 ns) with respect to the 326-nm pulse, and then separated into a pump and a probe beam of opposite polarization. P_{1-3} indicate the crossed polarizers that reduce the probe intensity, an etalon is used to reduce the probe bandwidth. The fluorescence decay of the excited $^3P_1$ and $^3S_1$ states is measured with a photomultiplier tube PMT 1. Pulse 1 and pulse 3 overlap spatially and are dispersed behind the cell by a prism. Only pulse 3 is detected by the photomultiplier tube PMT 2. Stray light from pulse 2 is blocked by the polarizer P_4 in front of PMT 2. In the laser oscillation experiment two cavity mirrors CM 1 and CM 2 are placed around the cavity. The cavity length is matched to the cavity length of the mode-locked Nd:YAG laser and the dye lasers.

V. ABSOLUTE GAS-DENSITY MEASUREMENT

The cadmium density inside the vapor cell is measured by a simple optical method. Consider an absorbing medium in a thin long cell of length L. The fluorescence intensity from absorbing atoms can be detected at position z, where z is the path length that the exciting beam has traveled through the medium, $0<z<L$. The fluorescence intensity at position z, $I_{\rm fl}(\rho,z)$ is proportional to the product of the atomic density, ρ, and the local light intensity. In the rate-equation regime this local intensity depends on z through Beer's law, so that

$$I_{\rm fl}(\rho,z) \propto \rho I_0 e^{-\sigma_\lambda \rho z}, \tag{8}$$

with I_0 the input intensity, and σ_λ the stimulated emission cross section of the atom-light interaction. The fluorescence intensity at position z as a function of the density reaches a maximum for a density such that z equals the $1/e$ decay length: $\rho = [\sigma_\lambda z]^{-1}$. At lower densities the decrease of available atoms reduces the fluorescence, at higher densities it is increased absorption of incoming light that reduces the fluorescence. The maximum signal can be found by tuning ρ (changing the temperature of the vapor cell) and the density is simply calculated from just z and σ_λ.

In our experiment the bandwidth of the pump pulses (30 GHz) is large compared to the inhomogeneous broadening ($\Delta\nu_{D1}=1.4$ GHz) so that Beer's law does not apply. The first pulse is weak, i.e., it excites only a small fraction of the ground state population to the $^3P_1$ state. In this case of weak, resonant excitation the absorption is easily calculated in the frequency domain [19,20]. The position-dependent fluence is

$$F(z)=\int_{-\infty}^{\infty} I(\nu,z)\,d\nu, \tag{9}$$

with $F(0)$ the initial fluence of about 1 μJ/(π mm^2). Each frequency component of the intensity decays exponentially:

$$I(\nu,z)=e^{-\sigma_1(\nu)\rho z} I(\nu,0), \tag{10}$$

with $I(\nu,0)$ the spectral fluence distribution at $z=0$, and $\sigma_1(\nu)$ the absorption cross section. The absorption cross section $\sigma_1(\nu)$ for a Doppler broadened line is [21]

$$\sigma_1(\nu)=\sqrt{\frac{\ln 2}{16\pi^3}}\frac{\lambda_1^2 A_{21}}{\Delta\nu_{D1}}\exp\left(-\frac{4\ln 2\,\nu^2}{\Delta\nu_{D1}^2}\right), \tag{11}$$

with A_{21} the Einstein A coefficient and $\Delta\nu_{D1}$ the full width at half maximum (FWHM) Doppler width. The density of excited $^3P_1$ atoms is now easily calculated from the spatial decay of the fluence:

$$n(z,\rho)=-\frac{dF(z)}{\varepsilon_1 dz}=\int_{-\infty}^{\infty}\sigma_1(\nu)\rho e^{-\sigma_1(\nu)\rho z} I(\nu,0)\,d\nu, \tag{12}$$

with ε_1 the photon energy at 326 nm. The function $n(z,\rho)$ has a maximum as a function of ρ, similar to the light intensity given in Eq. (8). In the actual experiment we optimized the fluorescence signal of the $^3P_1$ state at $z=L/2$ by adjusting the temperature. The resulting atomic density for $z=L/2=5$ cm is $\rho=3.1\times10^{13}$ cm^{-3}, based on $\lambda_1=326$ nm, and $A_{21}=(2.4\ \mu\text{s})^{-1}$. The $^3P_1$ excited-state population density in the middle of the cell as a function of atomic density is given in Fig. 4(a). The fluence of pulse 1 as a function of the position in the cell is depicted by the solid line in Fig. 4(b), the dotted line represents Beer's law of absorption for the same cross section and density. The excited-state population fraction as function of position in the cell is given in Fig. 4(c). [Both fluence and population fraction are calculated for the optimized atomic density obtained from Fig. 4(a).] Since the fraction of excited states decays almost exponentially along the cell, we will from now on assume pure exponential decay of the population fraction in the experiment:

$$\frac{N_{^3P_1}(z)}{N_{^3P_1}(0)}=e^{-2z/L}. \tag{13}$$

Based on the temperature of the oven of 225 °C, we expect a vapor pressure of 2.6×10^{-3} mbar or an atomic density of $\rho=3.8\times10^{13}$ cm^{-3}. This is in good agreement with the value based on the maximum fluorescence calculation, $\rho=3.1\times10^{13}$ cm^{-3}. In further calculations we will assume this latter density.

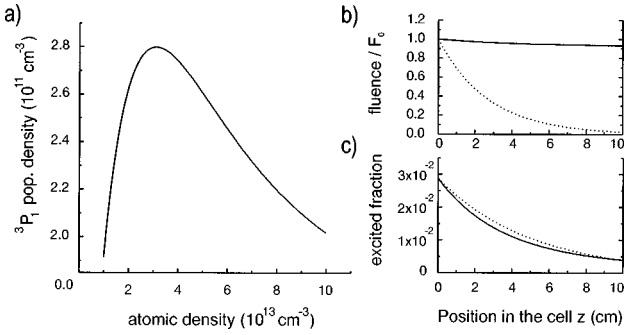

FIG. 4. (a) Population density of the $^3P_1$ state as a function of atomic density at $z=L/2=5$ cm, assuming a pulse energy of 1 μJ. The position of the maximum value, $\rho=3.1\times10^{13}$ cm^{-3} depends only on the cross section $\sigma_1(\nu)$. (b) Loss of fluence of pulse 1 as a function of position in the cell. The solid line is calculated for the experiment. The dotted line would be the result if Beer's law would apply, i.e., if the pulse were narrow band. (c) Position dependence of the excited $^3P_1$ population fraction. The solid line was calculated for the experiment, the dotted line gives a pure exponential decay proportional to $e^{-2z/L}$. This justifies our assumption that both excited-state population fractions $N_{^3P_1}(z)$ and $N_{^3S_1}(z)$ decrease from their initial value at $z=0$ by a factor e^{-1} halfway into the cell, and a factor e^{-2} at $z=L$.

The fluorescence signal of the $^3P_1$ state in a magnetic field of 6.25×10^{-5} T is given in Fig. 5. The figure shows the population oscillation between the coupled and noncoupled states, $|\phi_N\rangle$ and $|\phi_C\rangle$. These oscillations can only be seen in a direction perpendicular to the magnetic field, the observed phase of the oscillation depending on the position of the detector. The well-known analogy with a light house is applicable to the $^3P_1$ state atoms. The direction of the tower is parallel to the magnetic field lines, the rotation frequency of the light house is the frequency splitting caused by the magnetic field (Larmor frequency).

We have used the quantum-beat measurements to calibrate the magnetic field strength. Note that since the delay

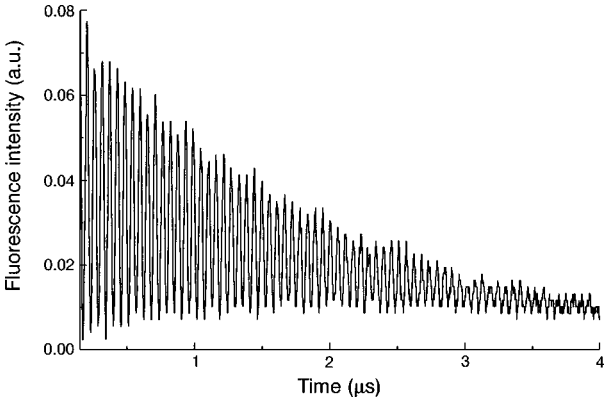

FIG. 5. The fluorescence intensity of the $^3P_1$ state in Cd in a magnetic field of $B=6.25\times10^{-5}$ T. This is a typical quantum beat picture showing a well defined coherence between the $^3P_1$ sublevels. Larmor frequencies from 2.4 MHz (Earth magnetic field) up to 140 MHz have been measured. The lifetime of the $^3P_1$ state is 2.4 μs.

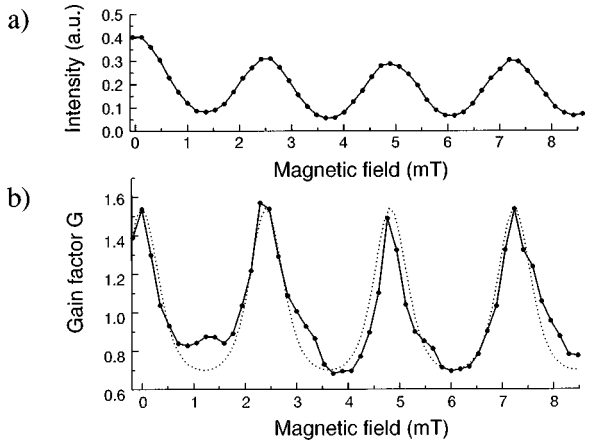

FIG. 6. (a) Fluorescence intensity of the $^3S_1$ state as a function of magnetic field. (b) Gain factor of the probe beam. The gain curve is more sharply peaked than the fluorescence curve, which has the expected cosine-squared shape. The photomultiplier signal was averaged over 100 shots per data point. The dotted line is a fitted curve. The fitted population parameters are $N_{^3P_1}(0)=7.3\times10^{-3}$, $N_{u,\max}(0)=3.3\times10^{-3}$.

time in our experiment is only 10 ns, Fig. 5 shows that the populations and coherences are preserved long enough for the gain experiments.

VI. PUMPING THE LASER TRANSITION

The second excitation pulse, promoting population from $|\phi_N\rangle$ to $|u\rangle$, arrives after a 10-ns delay with respect to the first pulse. During this delay the $^3P_1$ population oscillates between $|\phi_N\rangle$ and $|\phi_C\rangle$. Thus the amount of population pumped into the $^3S_1$ state by pulse 2 depends on the phase θ_L of the Larmor precession in the $^3P_1$ state. For example, if the $|\phi_N\rangle$ state is empty when pulse 2 arrives, there simply is no population to be transferred to the upper state. Thus, for a fixed delay, the population that is excited to the $^3S_1$ level depends on the Larmor frequency and varies as a cosine-squared function of the magnetic field,

$$N_u = N_{u,\max}\cos^2(\theta_L), \tag{14}$$

with $N_{u,\max}$ the maximum amount of $^3S_1$ population. In the experiment, N_u is monitored by measuring the fluorescence of the $|^3S_1\rangle\leftrightarrow|^3P_2\rangle$ transition at 508 nm; see Fig. 1. The fluorescence intensity is directly proportional to the population of the $^3S_1$ state and shows the expected cosine squared dependence as a function of magnetic field; see Fig. 6(a). The influence of shot-to shot fluctuations in intensity was reduced by averaging over 100 shots per magnetic field value.

In contrast to pulse 1, pulse 2 cannot be considered weak. The cross section for the second pump field (and probe pulse) at 479 nm is much larger than for the 326 nm transition, because it involves an optically allowed transition. In addition, the pulse energy at 479 nm is larger. For a bandwidth-limited pulse this would mean that an arbitrary fraction of the $^3P_1$ population could be transferred to the upper state, depending on the area of the pulse. However, the pulses in our experiment are not Fourier limited. The FWHM product of pulse duration (35 ps) and bandwidth (30 GHz) is

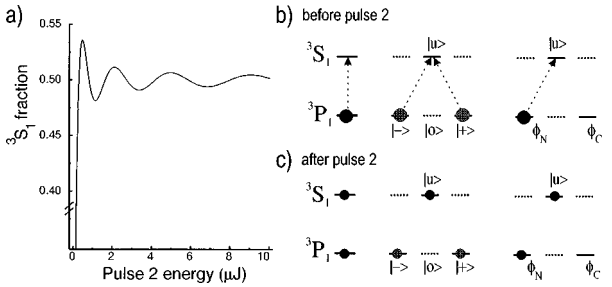

FIG. 7. (a) $^3S_1$ population as a fraction of the $^3P_1+^3S_1$ total population, plotted as a function of the pulse energy of pump pulse 2. (b) Populations before interaction with pump pulse 2. From left to right: level population, population in atomic eigenbasis and population in basis of superposition states. (c) Populations after interaction with pump pulse 2.

2.4 times larger than the smallest possible product (0.44) for a Gaussian pulse. Calculations based on the Bloch equations show that pulses with these characteristics and a fluence of a few times the equivalent 2π fluence excite within narrow margins (2%) exactly 50% to the excited state. This result is quite robust against variation of both the exact fluence and the duration-bandwidth product; see Fig. 7(a). The populations before and after interaction with pump pulse 2 are schematically indicated in Fig. 7(b) and Fig. 7(c), respectively.

The pulse energy of pulse 2 (10 μJ) is much larger than the total energy that can be absorbed by the excited $^3P_1$ atoms, $\rho V N_{^3P_1}\varepsilon_2\approx0.1$ μJ. Therefore the intensity of pulse 2 remains constant and we can assume the same position dependence of the $^3S_1$ population in the cell as for the $^3P_1$ population, illustrated in Eq. (13) and Fig. 4.

VII. GAIN MEASUREMENTS

In the following we describe how the absolute populations $\rho N_{^3S_1}$ and $\rho N_{^3P_1}$ can be determined, relying only on relative measurements, by a probe experiment using a third pulse, coupling the $|u\rangle\leftrightarrow|\phi_C\rangle$ transition.

The probe field (pulse 3) arrives immediately after the second excitation pulse ($\Delta\tau\approx0.2$ ns), and probes the $|u\rangle\leftrightarrow|\phi_C\rangle$ transition. The probe is amplified or absorbed according to the sign of the population difference on this transition,

$$\Delta N_{uc}(z,\theta_L) = N_{u,\max}(z)\cos^2(\theta_L) - N_{^3P_1}(z)\sin^2(\theta_L). \tag{15}$$

We discuss the gain for three different precession angles of the population in the $^3P_1$ state, $\theta_L=0$, $\pi/4$, $\pi/2$.

(i) $\theta_L=0$, $\Delta N_{uc}(0)=N_{u,\max}(0)$: maximum gain, the optically coupled $|\phi_C\rangle$ state is empty.

(ii) $\theta_L=\pi/4$, $\Delta N_{uc}(0)=\frac{1}{2}[N_{u,\max}(0)-N_{^3P_1}(0)]$: absorption because $N_{u,\max}(0)<N_{^3P_1}(0)$.

(iii) $\theta_L=\pi/2$, $\Delta N_{uc}(0)=-N_{^3P_1}(0)$: maximum absorption, the $^3S_1$ state is empty.

For instance, if the magnetic field is 1.2 mT, then $\theta_L=\pi/2$. When pulse 2 arrives the population in the $^3P_1$ state has completed one-half oscillation cycle in the superposition state basis leaving $|\phi_N\rangle$ empty. Therefore no population can

be excited to the $^3S_1$ state, resulting in a minimum of fluorescence intensity from this state, and absorption of the probe pulse; see Fig. 6.

In the measured gain curve as a function of magnetic field the peaks are narrower than the valleys; see Fig. 6(b). This asymmetry between observed absorption and emission is due to the exponential nature of the stimulated emission process which provides nonlinear gain, as will be explained in the following calculation.

To derive the gain for pulse 3 we need to determine the fluence fraction $F(L)/F(0)$ for the probe. This fraction cannot be calculated as simple as the absorption in Eq. (10) because ΔN_{uc}, the difference in population fraction between $|u\rangle$ and $|\phi_c\rangle$, is now position dependent: $\Delta N_{uc}=\Delta N_{uc}(z)$ according to Eq. (13)

$$\frac{\partial I(\nu,z)}{\partial z}=I(\nu,z)\sigma_2(\nu)\rho\Delta N_{uc}(0)e^{-2z/L} \tag{16}$$

giving

$$I(\nu,z)=\exp[\sigma_2(\nu)\rho\Delta N_{uc}(0)L\tfrac{1}{2}(1-e^{-2z/L})]I(\nu,0), \tag{17}$$

where $I(\nu,0)$ is the spectral fluence of the incident probe light. Its bandwidth is reduced in the experiment to 2 GHz, twice the Doppler width, using a high finesse 1-mm etalon, $R=0.95\%$ as a spectral filter. The cross section $\sigma_2(\nu)$ is calculated from Eq. (11), with $\lambda_2=479$ nm, $\Delta\nu_{D2}=1.0$ GHz, and $A_{32}=(3\times 10\ \text{ns})^{-1}$ (the factor 3 is a result of the three possible decay channels from the $^3S_1$ state; see Fig. 1). Using Eq. (9) the gain (or absorption) of the probe fluence $F(z)/F(0)$ can be calculated.

In the actual experiment not all the probe light interacts with the atoms, which we will incorporate with an overlap factor β. Light that does not interact with the atoms but does contribute to the signal of PMT 3 can be a result of, e.g., incomplete spatial overlap (various transverse profiles are involved, pump pulse 2 and probe pulse 3 make a small angle), or incomplete spectral overlap (not all shots hit atomic resonance). The observed gain curve can be reproduced using a simple model for the gain factor G incorporating position-dependent populations Eq. (13) and the overlap factor β:

$$\begin{aligned} G&=(1-\beta)+\beta\frac{F(L)}{F(0)}\\ &=(1-\beta)+\frac{\beta}{F(0)}\int_{-\infty}^{\infty}e^{\sigma_2(\nu)\rho\Delta N_{uc}(0)L1/2(1-e^{-2})}I(\nu,0)d\nu. \end{aligned} \tag{18}$$

To fit the model to the measured gain curve in order to obtain values for the population fractions $N_{u,\max}(0)$ and $N_{^3P_1}(0)$ we only need the cross sections $\sigma_1(\nu),\sigma_2(\nu)$ and the density ρ as input parameters.

The gain curve [Eq. (18) with Eq. (15)] is fitted to the data and we obtain the population fractions as fit parameters: $N_{^3P_1}(0)=7.3\times10^{-3}$, $N_{u,\max}(0)=3.3\times10^{-3}$, and $\beta=0.55$. This supports our assumption that half of the available $^3P_1$ population is excited to the $^3S_1$ state. For a fixed overlap factor β the upper state fraction $N_{u,\max}(0)$ is determined by the maximum gain and the lower state fraction $N_{^3P_1}(0)$ from the minimum of the gain curve. The overlap factor β was fitted to give the right asymmetry of the gain curve. Thus we have extracted absolute values for the populations and the density of the gain medium using only the measured shape of the gain curve and the optimization of the absorption of the first pulse to give maximum fluorescence half-way into the cell. Evidently, this procedure is also applicable for regular gain media with inversion.

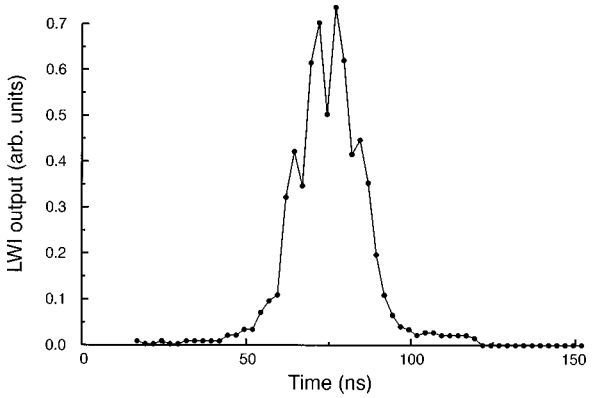

FIG. 8. Output of the mode-locked inversionless laser. The dots are the individual points as measured with a 300-MHz Lecroy 9450 oscilloscope. The magnetic field was switched off.

The gain curve in Fig. 6 shows a maximum gain of 1.5. This rather low amplification factor is due to instabilities in the Nd:YAG oscillator output, which lead to large pulse-to-pulse fluctuations in energy and spectral profile. The fluctuations in the population of the $^3S_1$ state cause fluctuations in the amplification of the probe beam. Larger gain factors of over a factor 10 have been measured in single-shot experiments. For these shots the overlap factor was optimal $\beta=1$ (spectral overlap) and both the populations and the inversion had above average values. Calculated following Eq. (18) this results in a population fraction $N_{u,\max}(0)=9\times10^{-3}$ and a maximum gain on line center of $\sigma_2(0)\rho N_{^3S_1}(0)=0.85$ cm^{-1}.

VIII. INVERSIONLESS LASER ACTION

In the final, laser-oscillation experiment we have blocked the probe pulse and introduced a laser cavity around the amplifying medium consisting of CM 1 and CM 2; see Fig. 3. The cavity length, 107 cm, was matched to the cavity length of the Nd:YAG oscillator and the dye lasers. The mirror CM 1 has a $R_1=90\%$ reflectance at 479 nm and is transparent for 326 nm. The outcouple mirror CM 2 has a $R_2=50\%$ reflectance at 479 nm. The first pump pulse remains unchanged. We replaced the second pump pulse by a pulse train, consisting of a train of five 35-ps pulses, of approximately 200 nJ each. Therefore the total energy in this second pumping step has been reduced by a factor of 10, as compared to the gain measurements of the previous section. The magnetic field was off in this experiment.

After alignment of the cavity mirrors a train of 479-nm pulses is detected on photomultiplier PMT 2. A typical result is given in Fig. 8. The output consists of a train of four pulses (the apparent temporal overlap of the output pulses is

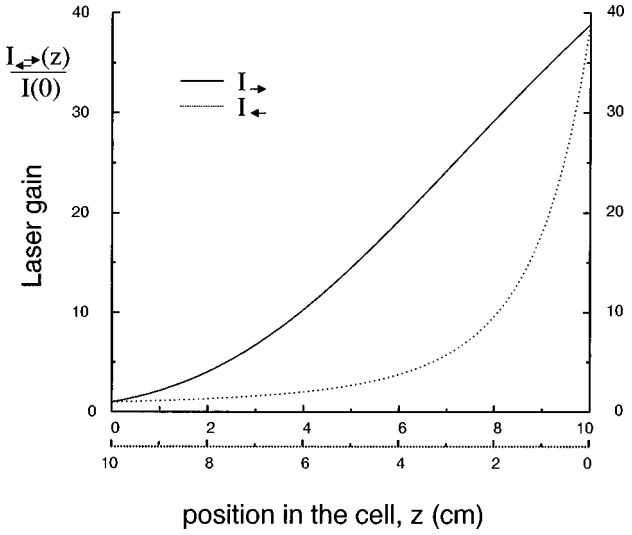

FIG. 9. Buildup of laser intensity in the gain medium. The solid line represents the buildup copropagating with the pump beams, the dotted line gives the buildup in the counterpropagating direction. The gain is calculated using Eq. (17) with $\nu=0$ and an excited-state population based on the single-shot experiments, $N_{u,\max}(0)=9\times10^{-3}$.

due to bandwidth limitations of the oscilloscope and the photomultiplier tube). The polarization of the detected laser light is linear and parallel to the polarization of the probe field in the gain experiment.

A few interesting observations can be made from Fig. 8. Because the number of output pulses is marginally smaller than the number of pump pulses and because the intensity of the consecutive pulses does not grow exponentially, we conclude that the laser saturates after just a few round trips. On the basis of the stimulated emission cross section we know that the saturation fluence is

$$F_{\mathrm{sat}}=\frac{hc}{\lambda_2\sigma_2(0)}, \tag{19}$$

giving a saturation energy of 4.3 nJ over a beam diameter of 2 mm. Thus the observed amplification from a single photon (spontaneous emission) to saturated output, 4.3 nJ, constitutes an amplification of 1×10^{10}.

In order to check the consistency of saturation energy, number of round trips, gain per round trip, and overall gain, we introduce the round-trip gain G_{rt}. First note that, although the upper state population of the laser reduces in the travel direction of the pump beams, the single-pass gain of the laser in the direction of the pump beams is equal to the gain in the counterpropagating direction, as is illustrated in Fig. 9. The round-trip gain factor is

$$G_{\mathrm{rt}}=R_1R_2(1-0.04)^{16}\left(\frac{I(\nu=0,z=L)}{I(\nu=0,z=0)}\right)^2, \tag{20}$$

where the equality of copropagating and counterpropagating single-pass gain is explicitly used. The gain factor $I(0,L)/I(0,0)$ is calculated from Eq. (17), thus assuming a resonant laser with a bandwidth smaller than the Doppler width $\Delta\nu_{D2}=1$ GHz. (This means that the pulse duration of the pulses in the laser oscillator train have a duration of at least 0.44 ns.) The loss factor $(1-0.04)^{16}$ is a result of the presence of two cell windows and two windows inside the oven which are passed two times per round trip. For the maximum gain as in Fig. 9 we know on the basis of Eq. (18) and Eq. (15) that $N_{u,\max}(0)=9\times10^{-3}$, leading to a maximum round-trip gain of $G_{\mathrm{rt}}=353$.

The amplification of 10^{10} from a single photon energy to the saturation energy, can be achieved in only a few round trips. Assuming a Gaussian envelope of the pump pulses (with 5 pulses above 25% of the peak value), a round-trip gain factor of $G_{\mathrm{rt}}=230$ will lead to a total gain of 10^{10} for the strongest peak under the envelope. Although only five pulses exceed 25% of the peak value, the preceding weak pulses (below 25%) play an important role in the buildup of the laser oscillations. The $^3S_1$ population needed for a round-trip gain $G_{\mathrm{rt}}=230$ can be calculated using Eq. (20) and Eq. (17), giving $N_{u,\max}(0)=8.5\times10^{-3}$.

On the one hand the gain experiments of the previous section resulted in an average upper-state population fraction of $N_{u,\max}(0)=3.2\times10^{-3}$. On the other hand the maximum gain measurement resulted in an upper-state population fraction of $N_{u,\max}(0)=9\times10^{-3}$. The value found in the lasing experiment is consistent with this interval and supports our assumptions concerning the small number of pulses needed to reach the low saturation energy.

IX. CONCLUSION

We have performed both amplification and laser-oscillation experiments in cadmium vapor. There is no inversion between any two levels in the system. Transforming to a basis of coupled and noncoupled states reveals a hidden inversion and allows us to make a two-level analysis of the experiment. A method based on a local maximum in fluorescence signal was used to calculate the atomic density. Using this density as an input parameter in a model for the gain, we extracted the population fractions of the laser levels involved and verified that there is no inversion in the atomic basis. Inversionless single-pass gains were measured. In addition, we obtained synchronously pumped inversionless laser operation.

ACKNOWLEDGMENTS

The work in this paper is part of the research program of the ''Stichting voor Fundamenteel Onderzoek van de Materie'' (Foundation for Fundamental Research on Matter), and was made possible by financial support from the ''Nederlandse Organisatie voor Wetenschappelijk Onderzoek'' (Netherlands Organization for the Advancement of Research). The research of R.S. has been made possible by the Royal Netherlands Academy of Arts and Sciences. The research of A.M. was part of the European Erasmus program for student exchange.

[1] O. A. Kocharovskaya and Y. I. Khanin, Pis'ma Zh. Eksp. Teor. Fiz. **48**, 581 (1988) [JETP Lett. **48**, 630 (1988)].
[2] M. O. Scully, S. Y. Zhu, and A. Gavrielides, Phys. Rev. Lett. **62**, 2813 (1989).
[3] S. E. Harris, Phys. Rev. Lett. **62**, 1033 (1989).
[4] A. Nottelmann, C. Peters, and W. Lange, Phys. Rev. Lett. **70**, 1783 (1993).
[5] E. S. Fry, X. Li, D. Nikonov, G. G. Padmabandu, M. O. Scully, A. V. Smith, F. K. Tittel, C. Wang, S. R. Wilkinson, and S. Y. Zhu, Phys. Rev. Lett. **70**, 3235 (1993).
[6] W. E. van der Veer, R. J. J. van Diest, A. Dönszelmann, and H. B. van Linden van den Heuvell, Phys. Rev. Lett. **70**, 3243 (1993).
[7] J. A. Kleinfeld and A. D. Streater, Phys. Rev. A **49**, R4301 (1994).
[8] J. A. Kleinfeld and A. D. Streater, Phys. Rev. A **53**, 1839 (1996).
[9] A. S. Zibrov, M. D. Lukin, D. E. Nikonov, L. W. Hollberg, M. O. Scully, V. L. Velichansky, and H. G. Robinson, Phys. Rev. Lett. **75**, 1499 (1995).
[10] G. G. Padmabandu, G. R. Welch, I. N. Shubin, E. S. Fry, D. E. Nikonov, M. D. Lukin, and M. O. Scully, Phys. Rev. Lett. **76**, 2053 (1996).
[11] O. A. Kocharovskaya, Phys. Rep. **219**, 175–190 (1992).
[12] M. O. Scully, Phys. Rep. **219**, 191 (1992).
[13] P. Mandel, Contemp. Phys. **34**, 235 (1993).
[14] E. Arimondo, in *Progress in Optics*, edited by E. Wolf (North-Holland, Amsterdam, 1996), Vol. XXXV, Chap. V, pp. 258–354.
[15] F. B. de Jong, R. J. C. Spreeuw, and H. B. van Linden van den Heuvell, Phys. Rev. A **55**, 3918 (1997).
[16] A. Lezama, Yifu Zhu, Manoj Kanskar, and T. W. Mossberg, Phys. Rev. A **41**, 1576 (1990).
[17] T. W. Hänsch and P. Toschek, Z. Phys. **236**, 213 (1970).
[18] G. Petite, P. Agostini, and C. K. Wu, Rev. Phys. Appl. **20**, 527 (1985).
[19] M. D. Crisp, Phys. Rev. A **1**, 1604 (1970).
[20] L. Allen and J. H. Eberly, *Optical Resonance and Two-Level Atoms* (Dover, New York, 1987).
[21] W. T. Silfvast, *Laser Fundamentals* (Cambridge University Press, Cambridge, 1996).